To be published in *Journal of Geophysical Research* around May 2000.

Alfvénic collisionless magnetic reconnection and the Hall term

M. A. Shay, J. F. Drake, and B. N. Rogers
Institute for Plasma Research, University of Maryland, College Park

R. E. Denton
Department of Physics and Astronomy, Dartmouth College, Hanover, New Hampshire

Abstract

The Geospace Environment Modeling (GEM) Challenge Harris current sheet problem is simulated in 2 1/2 dimensions using full particle, hybrid, and Hall MHD simulations. The same gross reconnection rate is found in all of the simulations independent of the type of code used, as long as the Hall term is included. In addition, the reconnection rate is independent of the mechanism which breaks the frozen-in flux condition, whether it is electron inertia or grid scale diffusion. The insensitivity to the mechanism which breaks the frozen-in condition is a consequence of whistler waves, which control the plasma dynamics at the small scales where the ions become unmagnetized. The dispersive character of whistlers, in which the phase velocity increases with decreasing scale size, allows the flux of electrons flowing away from the dissipation region to remain finite even as the strength of the dissipation approaches zero. As a consequence, the throttling of the reconnection process as a result of the small scale size of the dissipation region, which occurs in the magnetohydrodynamic model, no longer takes place. The important consequence is that the minimum physical model necessary to produce physically correct reconnection rates is a Hall MHD description which includes the Hall term in Ohm's law. A density depletion layer, which lies just downstream from the magnetic separatrix, is identified and linked to the strong in-plane Hall currents which characterize kinetic models of magnetic reconnection.

1. Introduction

Magnetic reconnection plays an important role in the dynamics of the magnetosphere, the solar corona, and laboratory experiments by allowing magnetic energy to be released in the form of high-velocity streams of electrons and ions. In a sufficiently collisional plasma, resistive MHD theory is valid for determining the reconnection rate. In this regime, however, the dissipation region forms a macroscopic Sweet-Parker current sheet which severely limits the reconnection rate due to the Alfvén limit on the outflowing ions region [*Sweet,* 1958; *Parker,* 1957; *Biskamp,* 1986]. The inflow of ions into the dissipation region scales like

$$v_{\rm in} \sim \frac{\delta}{L} c_A \ll c_A, \tag{1}$$

where δ and L are, respectively, the width and length of the dissipation region and c_A is the Alfvén speed. As resistivity goes to zero, $\delta \to 0$ and reconnection proceeds only in the presence of anomalous resistivity [*Biskamp and Bremer,* 1993]. In physical systems of interest, classical resistivity is too weak to explain the observations, and anomalous resistivity remains poorly understood.

In collisionless plasma the dissipation region develops a multiscale structure based on electron and ion scale lengths [*Biskamp et al.,* 1997; *Shay et al.,* 1998]. These scales can be obtained from the kinetic Ohm's law [*Vasyliunas,* 1975]:

$$\frac{4\pi}{\omega_{pe}^2}\frac{d\mathbf{J}}{dt} = \mathbf{E} + \frac{1}{c}\mathbf{v}\times\mathbf{B} - \frac{1}{nec}\mathbf{J}\times\mathbf{B} + \frac{1}{ne}\nabla\cdot\vec{\mathbf{P}}_e - \eta\mathbf{J}, \tag{2}$$

where $\vec{\mathbf{P}}_e$ is the electron pressure tensor, n is the number density, and e and c are the elementary charge and speed of light, respectively. Equation (2) is simply the electron equation of motion rewritten in terms of the traditional MHD terms ($\mathbf{E}$ and $\mathbf{v}\times\mathbf{B}$) plus the Hall ($\mathbf{J}\times\mathbf{B}$), pressure and electron inertial terms. At scale lengths greater than the ion inertial length, $\delta_i \equiv c/\omega_{pi}$, all of the terms in (2) except the MHD terms can be neglected and MHD remains a valid description of the plasma dynamics. In the weak axial field limit of interest here, within a distance from the x line of the order of δ_i, the ion motion decouples from that of the electrons as a result of the Hall term in (2) [*Sonnerup,* 1979; *Terasawa,* 1983]. In this region of scale-size δ_i, the ions are accelerated away from the x line, eventually reaching the Alfvén velocity. Within this ion inertial region but outside of an electron inertial region, the electrons remain frozen-in to the magnetic field, and the dynamics of the electron magnetofluid are described by a set of nonlinear whistler equations [*Mandt et al.,* 1994; *Biskamp et al.,* 1997]. In this region the $\mathbf{E}$ and $\mathbf{J}\times\mathbf{B}$ terms dominate the kinetic Ohm's law. Finally, even closer to the x line, the electrons decouple from the magnetic field owing to their finite thermal velocity [*Laval et al.,* 1966] or their convective motion [*Dungey,* 1988; *Burkhart et al.,* 1990]. In a fluid description the mechanism for breaking the electron frozen-in condition can be described either as electron inertia ($d\mathbf{J}/dt$ in (2)) or as a nongyrotropic pressure ($\nabla\cdot\vec{\mathbf{P}}_e$ in (2)) [*Vasyliunas,* 1975] and has recently been the subject of intense scrutiny [*Lyons and Pridemore-Brown,* 1990; *Cai et al.,* 1994; *Biskamp et al.,* 1997; *Horiuchi and Sato,* 1997; *Shay et al.,* 1998; *Kuznetsova et al.,* 1998; *Hesse and Winske,* 1998]. Studies examining the impact of electron dynamics on the rate of reconnection have, however, found that after reconnection has entered the nonlinear regime, the process which breaks the frozen-in constraint for the electrons has no effect on the reconnection rate [*Biskamp et al.,* 1997; *Shay and Drake,* 1998; *Hesse et al.,* 1999]. In particular, the width of the region over which the frozen-in constraint is broken no longer limits the reconnection rate as it does in the resistive MHD case. The presence of the Hall term proportional to $\mathbf{J}\times\mathbf{B}$ in the generalized Ohm's law and the associated dynamics of whistler waves provide the essential physics required to obtain this result.

At a phenomenological level, the acceleration of plasma transverse to the magnetic field is limited by the phase speed of the waves which characterize the acceleration process. In the case of MHD this corresponds to the Alfvèn speed. At the small scales where the electron frozen-in condition is broken, the electron and ion motion decouples, and the waves which characterize the transverse dynamics of electrons are whistler waves, with the quadratic dispersion character, $\omega \sim k^2$. The wave speed of the whistler and therefore the maximum outflow speed of the electrons is given by $v \sim k \sim 1/\delta$, where δ is the transverse width of the current layer. The result is that the electron flux out of the dissipation region, proportional to $v\delta$, can remain independent of δ as $\delta \to 0$. On a more quantitative level, the strongly bent, newly reconnected field lines basically form a standing whistler wave. As in a conventional whistler, the self-consistent out-of-plane current rotates this

bent magnetic field out of the plane of the reconnection, producing the characteristic self-generated quadrupole out-of-plane magnetic field which characterizes kinetic reconnection. At the same time the electron flow (current) driven at the x line owing to the reconnection electric field rotates into the outflow direction so that the electron outflow velocity $v_{\rm out}$ is given by

$$v_{\rm out} \sim J/ne \sim cB/(4\pi ne\delta). \quad (3)$$

Again, the flux $\delta v_{\rm out}$ can therefore remain finite even in the limit that δ becomes very small so that the mechanism which breaks the frozen-in condition does not limit the electron flux out from the dissipation region.

Because the electron dissipative dynamics do not constrain the rate of reconnection, the ions with their much larger mass ultimately limit the rate. Again, the Hall term plays a key role. The width of the ion outflow channel from the region around the x line scales like δ_i. Continuity of the flow of ions into and out of the dissipation region then yields the ion inflow velocity,

$$v_{\rm in} \sim \frac{\delta_i}{L} c_A. \quad (4)$$

The fact that the width of the ion outflow channel greatly exceeds the width of the electron dissipation scale already implies that kinetic reconnection rates can greatly exceed the conventional MHD model. In addition, however, the length L of the region downstream of the x line required to accelerate the ions up to the Alfvèn speed, which is macroscopic in the MHD system, remains microscopic in kinetic reconnection. Again, it is the dynamics of the whistler which facilitates the strong acceleration of the ions. The standing whistler, as it rotates the reconnected magnetic fields out of the plane of reconnection, rotates the reconnection electric field into the plane of reconnection and in particular toward the downstream direction. This large electric field accelerates the ions up to the Alfvèn speed over a distance of order $\sim 10\delta_i$. The rate of reconnection given in (4) therefore remains Alfvènic even in large systems where the system size is much greater than c/ω_{pi} [*Shay et al.*, 1999].

Therefore the inclusion of the Hall effect in the kinetic Ohm's law and the associated dynamics of whistlers, which occurs at spatial scales at and below c/ω_{pi} is the key to achieving fast reconnection in collisionless plasmas. A fundamental question which arises from these ideas is what is the minimal physics model required to simulate collisionless magnetic reconnection in the space physics environment? Once the minimum physics needed for a model to correctly model magnetic reconnection is determined, the essential physics can be incorporated into the next generation of large-scale models of space plasma systems such as the magnetosphere and the Sun. To this end, we have explored magnetic reconnection in a Harris current sheet using a variety of 2 1/2 dimensional simulation models, including full particle, hybrid with electron inertia, and Hall MHD with and without electron inertia. We find the following:

1. Full particle, hybrid, and even Hall MHD codes with no electron inertia produce the essentially identical reconnection rates. Therefore two fluid simulations with the Hall term may be adequate to produce realistic reconnection rates in large-scale simulations of magnetospheric phenomena.

2. During Alfvénic, whistler-mediated reconnection, the mechanism which breaks the frozen-in condition does not control the rate of magnetic reconnection.

3. A spatially constant resistivity is insufficient to balance the reconnection electric field in simulations of whistler-mediated reconnection. As a consequence, the electrons will become unmagnetized at the grid scale, with numerical diffusion balancing the reconnection electric field. In order to resolve the inner electron current sheet using a resistive model, a current dependent resistivity or some other higher-order resistivity is needed.

4. The loops of in-plane current which form during whistler-mediated reconnection drag the magnetic field in such a way that bands of increased magnetic pressure form along the separatrices. This increased magnetic pressure expels the unmagnetized ions and creates a "density depletion layer" along the separatrices.

2. Models

2.1. Hall MHD Simulation Model

The equations used to complete the Hall MHD simulations are as follows:

$$\frac{\partial n}{\partial t} = -\nabla\cdot\mathbf{J}_i, \quad (5)$$

$$\frac{\partial \mathbf{J}_i}{\partial t} = -\nabla\cdot(\mathbf{J}_i\mathbf{J}_i/n) + \mathbf{J}\times\mathbf{B} - \frac{1}{n}\nabla(P_i + P_e), \quad (6)$$

$$\frac{\partial P_i}{\partial t} = -\frac{\mathbf{J}_i}{n}\cdot\nabla P_i - \gamma P_i \nabla\cdot\frac{\mathbf{J}_i}{n}, \tag{7}$$

$$\frac{\partial P_e}{\partial t} = -\mathbf{u}_e\cdot\nabla P_e - \gamma P_e \nabla\cdot\mathbf{u}_e, \tag{8}$$

$$\frac{\partial \mathbf{B}'}{\partial t} = -\nabla\times\mathbf{E}', \tag{9}$$

$$\mathbf{E}' = \frac{\mathbf{J}}{\mathbf{n}}\times\mathbf{B}' - \frac{\mathbf{J}_i}{n}\times\mathbf{B} - \frac{1}{n}\nabla P_e, \tag{10}$$

$$\mathbf{B}' = (1-\delta_e^2\nabla^2)\mathbf{B}, \;\; \mathbf{J} = \nabla\times\mathbf{B}, \tag{11}$$

where $\gamma = 5/3$, $\mathbf{J}_i \equiv$ ion flux, $\mathbf{u}_e = \frac{1}{n}(\mathbf{J}_i - \mathbf{J}) =$ electron velocity, $P_e =$ electron pressure, $P_i =$ ion pressure, and $\delta_e \equiv c/\omega_{pe}$. Time has been normalized to $t_o = \Omega_i^{-1} = (eB_o/m_i c)^{-1}$, with B_o chosen as the initial lobe magnetic field. Length has been normalized to $L_o = c/\omega_{pi} = c\sqrt{m_i/(4\pi n_o e^2)}$, with n_o equal to the initial current sheet density minus the lobe density. The velocities therefore are normalized to the Alfvén velocity. We also assume quasi-neutrality: $n_i \approx n_e$. The above equations form a closed set. In Ohm's law in (10) the $\mathbf{J}/n\times\mathbf{B}'$ term produces the Hall effect and introduces the scale length c/ω_{pi} into the equations. This scale does not appear explicitly because it has been absorbed into the normalization. This term as well as the $\nabla P_e/n$ term is absent in MHD. The electron inertia, or electron mass, in Ohm's law manifests itself through the term proportional to δ_e^2 in the definition of $\mathbf{B}'$. In normalized coordinates, $\delta_e = \sqrt{m_e/m_i}$ and is treated as a spatially constant free parameter. At the end of each time step, $\mathbf{B}$ is unfolded from $\mathbf{B}'$ using fast Fourier transforms.

Because c/ω_{pe} in reality has a dependence on density, treating δ_e as a spatially constant parameter leads to an artificial thinning of the electron current sheet by a factor of 2 in the hybrid and Hall MHD simulations compared with the full particle model. Since this study is primarily focused on the minimum physics necessary to get realistic reconnection rates, this thinning can be considered a further test of the hypothesis that the reconnection rate is unaffected by the specifics of the electron dissipation.

A sixth-order k space diffusion is added to (9) to prevent energy from piling up at the grid scale. Because of the high order of the operator, it is negligible at the physical scales in the system. The strong depletion of the density just downstream of the separatrix (associated with in-plane Hall currents) created numerical problems which required the addition of second-order diffusion to (5), (7), and (8) to keep the pressures and densities from going negative. The results were cross-checked to insure that this diffusion did not affect the reconnection rates. The "density depletion layer" will be defined and discussed later in this paper.

2.2. Hybrid Simulation Model

The hybrid simulation model is very similar to the Hall MHD model, except that the ions are now treated as particles. The fluid equations that are evolved are unchanged from those in (8)-(11).

The equations used to step forward the particles are

$$\frac{d\mathbf{x}_i}{dt} = \mathbf{v}_i, \tag{12}$$

$$\frac{d\mathbf{v}_i}{dt} = \mathbf{E}'' + \mathbf{v}_i\times\mathbf{B}, \tag{13}$$

where $\mathbf{x}_i$ and $\mathbf{v}_i$ are the position and velocity of the ith ion particle and $\mathbf{E}'' = -\mathbf{u}_e\times\mathbf{B} - \frac{1}{n}\nabla P_e$. Note that we neglect the finite electron inertial correction to the electric field which is used to step the ions forward in time because this correction only becomes important at spatial scales of c/ω_{pe}. Changes in the electric field over a distance of c/ω_{pe} have very little effect on the motion of the ions because of their large mass. Because whistler waves in the electron fluid have a much higher velocity than waves associated with the ions, the time step for the fluid is taken to be much smaller than that of the ions [*Mandt et al.*, 1994], the fluid time step being typically 1/50 to 1/100 of the ion particle time step. At the end of each ion time step, the ion moments on a grid cell are determined by adding density and flux from each nearby particle.

2.3. Full Particle Model

The full particle model is fully electromagnetic; that is, it includes light waves and plasma oscillations. The field equations for this code are

$$\frac{\partial \mathbf{B}}{\partial t} = -\nabla\times\mathbf{E}, \tag{14}$$

$$\frac{\partial \mathbf{E}}{\partial t} = \overline{c}^2\left[\nabla\times\mathbf{B} - \mathbf{J}_i + \mathbf{J}_e\right], \tag{15}$$

where $\mathbf{J}_i$ and $\mathbf{J}_e$ are the ion and electron bulk currents which are determined by summing the individual particles onto the grid. The normalizations are the same as for the hybrid and Hall MHD codes, and $\overline{c}$ is the normalized speed of light: $\overline{c} \equiv c/(L_o/t_o) = c/c_A$.

The individual particle equations of motion are

$$\frac{d\mathbf{x}_{\mathbf{i}j}}{dt} = \mathbf{v}_{\mathbf{i}j}, \tag{16}$$

$$\frac{d\mathbf{v}_{\mathbf{i}j}}{dt} = \left[\mathbf{E} + \mathbf{v}_{\mathbf{i}j} \times \mathbf{B}\right], \tag{17}$$

$$\frac{d\mathbf{x}_{\mathbf{e}j}}{dt} = \mathbf{v}_{\mathbf{e}j}, \tag{18}$$

$$\frac{d\mathbf{v}_{\mathbf{e}j}}{dt} = -\frac{1}{m_e/m_i}\left[\mathbf{E} + \mathbf{v}_{\mathbf{e}j} \times \mathbf{B}\right], \tag{19}$$

where $\mathbf{x}_{\mathbf{i}j}$ and $\mathbf{v}_{\mathbf{i}j}$ are the position and velocity of the jth ion particle. The particle electron positions and velocities are denoted similarly. The values of $\mathbf{E}$ and $\mathbf{B}$ at the location of each particle are interpolated from nearby grid points. Because grid-scale electron plasma oscillations have a smaller frequency than grid-scale light waves, the field can be sub-stepped. For the simulations presented in this paper $\overline{c} = 25$, and there are six field times steps for every particle time step.

3. Initial Conditions

The initial conditions are described in detail in the introductory paper of the Geospace Environment Modeling (GEM) challenge project. Briefly, this study examines the dynamics of the reconnection of a Harris current sheet with a background lobe density of 0.2. The simulations are 2 1/2 dimensional and the simulation size is 25.6×12.8 in normalized coordinates. The boundary conditions are periodic along the x direction, with conducting walls along the z direction so that no flux can enter or leave through the z direction. A small magnetic perturbation is included in the initial conditions to form an initial magnetic island. However, The perturbation is large enough that random perturbations associated with the particle simulations will not change the location of the x line significantly, allowing easy comparison between Hall MHD, hybrid, and full particle simulations. The intent is for the system to be in a nonlinear regime from the outset so the differing growth rates of the linear tearing mode in the various models do not obscure the underlying common nonlinear physics.

4. Results

Figure 1 is a plot of the reconnected flux, that is, the integrated magnetic flux ψ between the x line and the o line, versus time for the three types of simulations done in this study: full particle, hybrid, and Hall MHD. All three simulations have $m_e/m_i = 1/25$ on a 512×256 grid. The slope of these lines gives the reconnection rate, which is equal to E_y. In all three cases, the reconnection proceeds very slowly until about $t \approx 10\,\Omega_i^{-1}$, when the reconnection rate sharply accelerates. The sharp increase of the reconnection rate has been observed in other simulations of reconnection [*Horiuchi and Sato,* 1997; *Ma and Bhattacharjee,* 1996]. The reconnection then proceeds at a relatively steady rate until the island saturates.

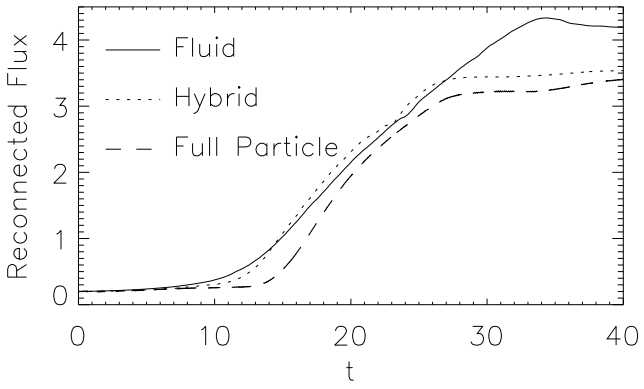

Figure 1. Reconnected magnetic flux (ψ/ψ_o) versus time for full particle, hybrid, and Hall MHD simulations, where $\psi_o \equiv B_o L_o$, and B_o and L_o are the normalization magnetic field and length scale.

All of the simulations in Figure 1 have the same parameters and the electron inertia is the same. The type of model used does not have a substantial impact on the gross reconnection rates observed, although there are some subtle differences. For example, the full particle simulation takes longer for the onset of reconnection, and the Hall MHD simulation reconnects more flux before saturating.

Figure 2 is a plot of various moments of a hybrid run with $m_e/m_i = 1/100$ on a 1024×512 grid at $t = 20\Omega_i^{-1}$. At this point in time, the amount of normalized flux that has reconnected is $2.0\psi_o$, where

$\psi_o \equiv B_o L_o$, and B_o and L_o are the normalization magnetic field and length scale. The simulation domain actually extends to $z = \pm 6.4$. The x line structure is clearly visible in Figure 2a, which is a contour plot of magnetic flux ψ, whose contours are parallel to the in-plane magnetic field lines. Here ψ is defined such that $\mathbf{B}_\perp = \hat{\mathbf{y}} \times \nabla\psi$, where the $\perp$ denotes in-plane components. Magnetic flux reconnects at the x line near $(x, z) = (0, 0)$ and forms flux bubbles around the o lines near $(x, z) = (\pm 12.8, 0)$, which expand outward and compress the magnetic flux against the reflecting walls at $z = \pm 6.4$. The in-plane ion flow is consistent with this motion of the fields lines, as seen in Figure 2b. The ions flow inward toward the x lines along the z direction and then are accelerated along the outflow direction, which is along x. Not all of the ions pass through the region close to the x line before accelerating along x. Many are accelerated along x by shock-like structures near the separatrices.

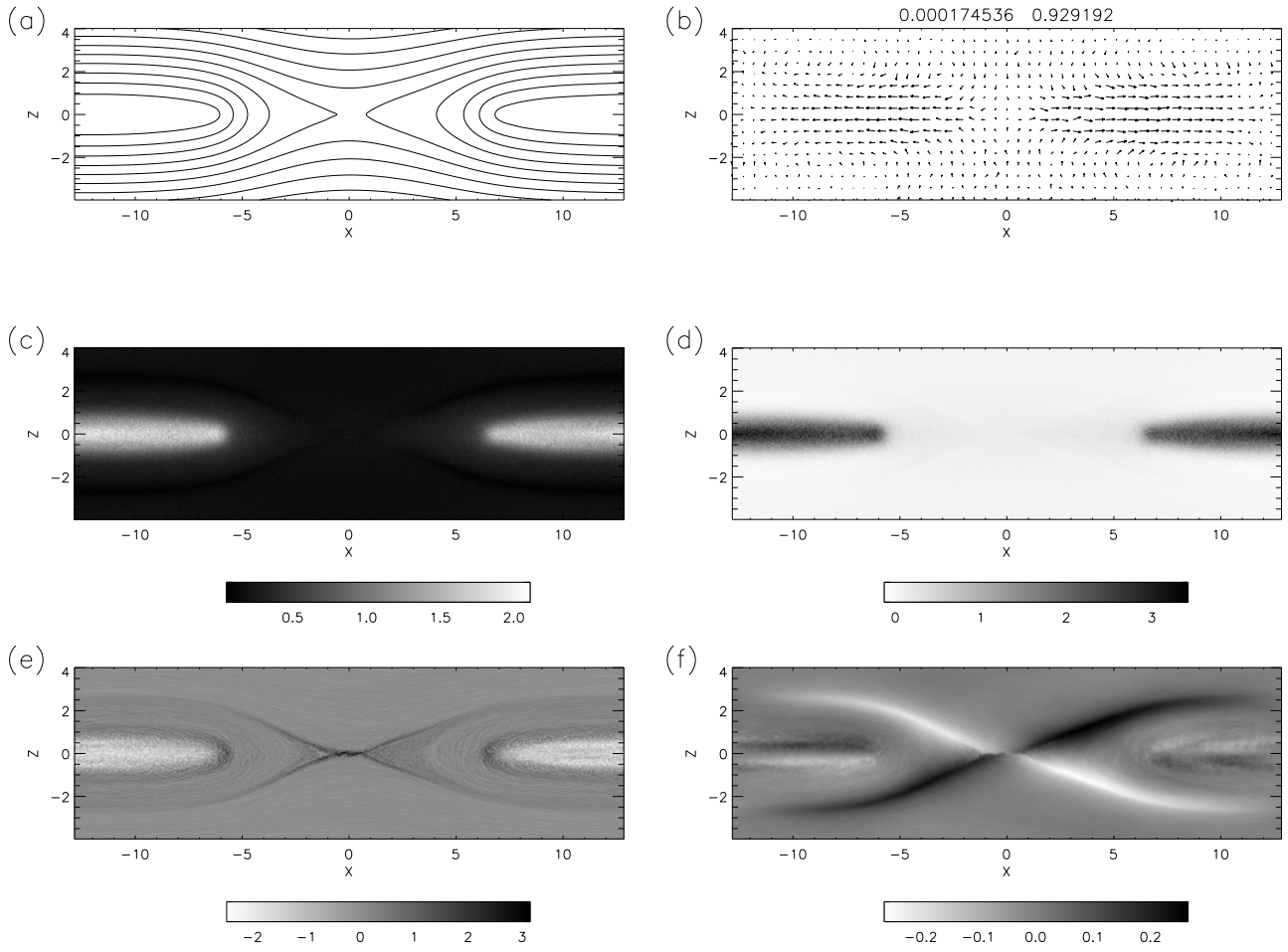

Figure 2. Results from a hybrid run with $m_e/m_i = 1/100$: (a) Magnetic field lines, (b) ion in-plane flows, (c) density, (d) ion out-of-plane current, (e) electron out-of-plane current, and (f) out-of-plane magnetic field.

Figure 2c is a plot of the density. At this time, all of the flux associated with the initial high-density current sheet has reconnected and flowed into the flux bubbles around the o line. The reconnecting plasma now has a much lower density. Almost all of the current at the x line is carried by the electrons, as shown in Figures 2d and Figures 2e, which are plots of the ion and electron out-of-plane currents, respectively. The only noticeable ion current is in the flux bubbles around the o line and is left over from the initial conditions. The electron current near the x line has very fine-scale structure at scales of the electron skin depth, c/ω_{pe}. Very close to the x line, there is a very thin electron current sheet slightly elongated along the x direction. Farther away from the x line, this current sheet splits into wings which basically map out the separatrices. Owing to the Hall term, which becomes important at scales $\leq c/\omega_{pi}$, the physics of whistlers become important in the region near the x line. This whistler physics induces out-of-plane magnetic fields, which take on a quadrupole structure as shown in Figure 2f [*Sonnerup,* 1979; *Terasawa,* 1983; *Mandt et al.,* 1994].

5. Role of the Electrons

Although the ions become unmagnetized at scale lengths below c/ω_{pi}, the electrons remain frozen-in until much smaller scales because of their smaller mass and thus smaller effective Larmor radius. In a fluid description of the electrons with scalar pressure and no large axial field, the frozen-in constraint is finally broken and magnetic topology is allowed to change when the scale sizes in the system approach c/ω_{pe}. Changing the electron mass therefore has the effect of changing this scale size. However, owing to the physics introduced with the Hall term in Ohm's law, neither the electron mass nor the physical model used to describe the electron dissipation has any effect on the gross reconnection rate. Although the reconnection rate stays the same, the dynamics of the electrons can change significantly depending on the physical model used, as will be shown in this section.

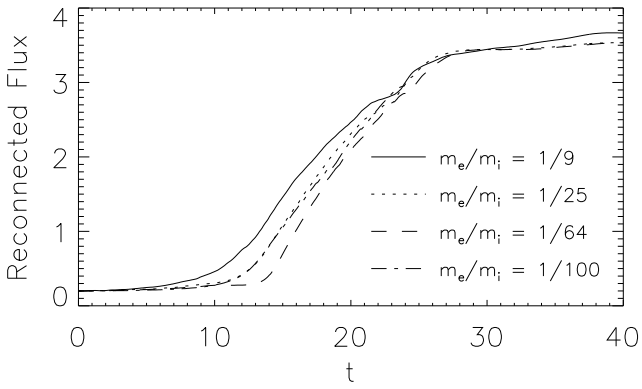

Figure 3. Reconnected magnetic flux (ψ/ψ_o) versus time for hybrid simulations with different values of m_e/m_i.

Figure 3 is a plot of the reconnected flux versus time for four different values of the electron mass. The electron to ion mass ratio is varied from 1/9 to 1/100, with little effect on the gross reconnection rate. This change in the electron mass does have a large affect on the electron dynamics at small scales, however, as is shown in Figure 4, which contains plots of electron out-of-plane current for two different electron masses. Both of these plots are taken at a time when 2.0 ψ_o of magnetic flux has reconnected. Figure 4a is a hybrid simulation with $m_e/m_i = 1/100$ (the same plot as Figure 2e), and Figure 4b is a hybrid run with the same parameters except $m_e/m_i = 1/9$ on a 512×256 grid. The thin current sheet near the x line is significantly broader in both the x and z directions in the case where m_e is larger. The wings of current which fan out from this current sheet also broaden when m_e is increased.

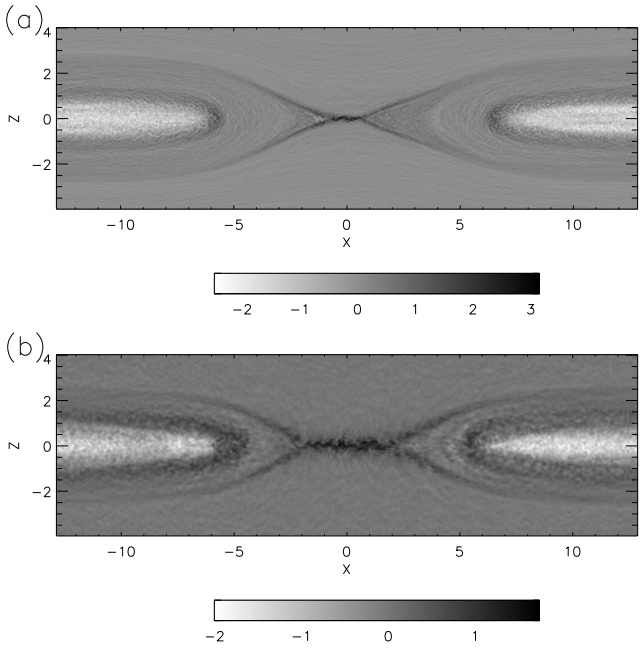

Figure 4. The electron out-of-plane current for hybrid simulations with (a) $m_e/m_i = 1/100$ and (b) $m_e/m_i = 1/9$.

In the limit of zero electron mass, the scale size of the electron layer in these simulations is determined by a hyper-resistivity (sixth-order dissipation in the magnetic field equation). The reconnection rate, however, remains unchanged from the case with finite electron mass. Figure 5 is a plot of the reconnected flux versus time for two Hall MHD simulations, one with $m_e/m_i = 1/25$ and one with $m_e/m_i = 0$. Both simulations are on a 512×256 grid. Although the run with $m_e/m_i = 0$ requires more time before the sharp onset of fast reconnection occurs, the two runs have virtually identical maximum reconnection rates and saturation values of reconnected flux.

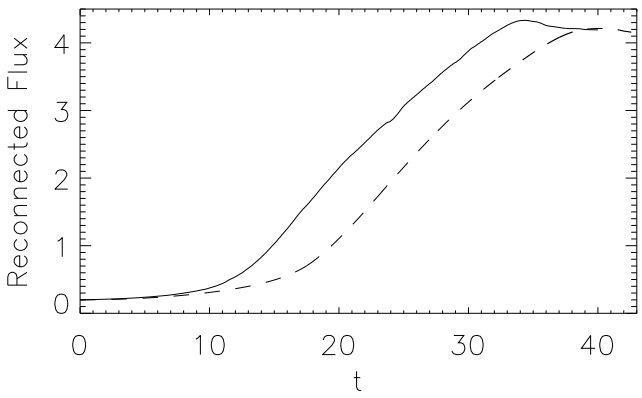

Figure 5. Reconnected magnetic flux (ψ/ψ_o) versus time for Hall MHD simulations: $m_e/m_i = 1/25$ (solid line) and $m_e/m_i = 0$ (dotted line).

It was shown in section 4 that the type of simulation used does not change the gross reconnection rate significantly. The electron response at small scales, however, can be very different depending on the model. In Figure 6, the electron out-of-plane current is plotted for the different types of simulations in this study: (Figure 6a) hybrid $m_e/m_i = 1/25$, (Figure 6b) Hall MHD $m_e/m_i = 1/25$, (Figure 6c) Hall MHD $m_e/m_i = 0$, and (Figure 6d) full particle $m_e/m_i = 1/25$. All plots are taken at times when $2.0\psi_o$ of magnetic flux has reconnected and all the simulations are on a 512×256 grid. The hybrid and Hall MHD cases with nonzero electron mass, Figures 6a and 6b, have central electron current sheets which are about the same size. The intensity of electron current density at the x line is also the same. In Figure 6c where $m_e = 0$, however, this current sheet has collapsed down to the grid scale in both directions, and the current at the x line is much larger. In addition, the small-scale fluctuations in the downstream region, present in all of the cases with finite electron mass, are absent. These fluctuations are believed to be caused by the electron inertia convective term in Ohm's law, which introduces shear flow instabilities into the problem [*Drake et al.,* 1997].

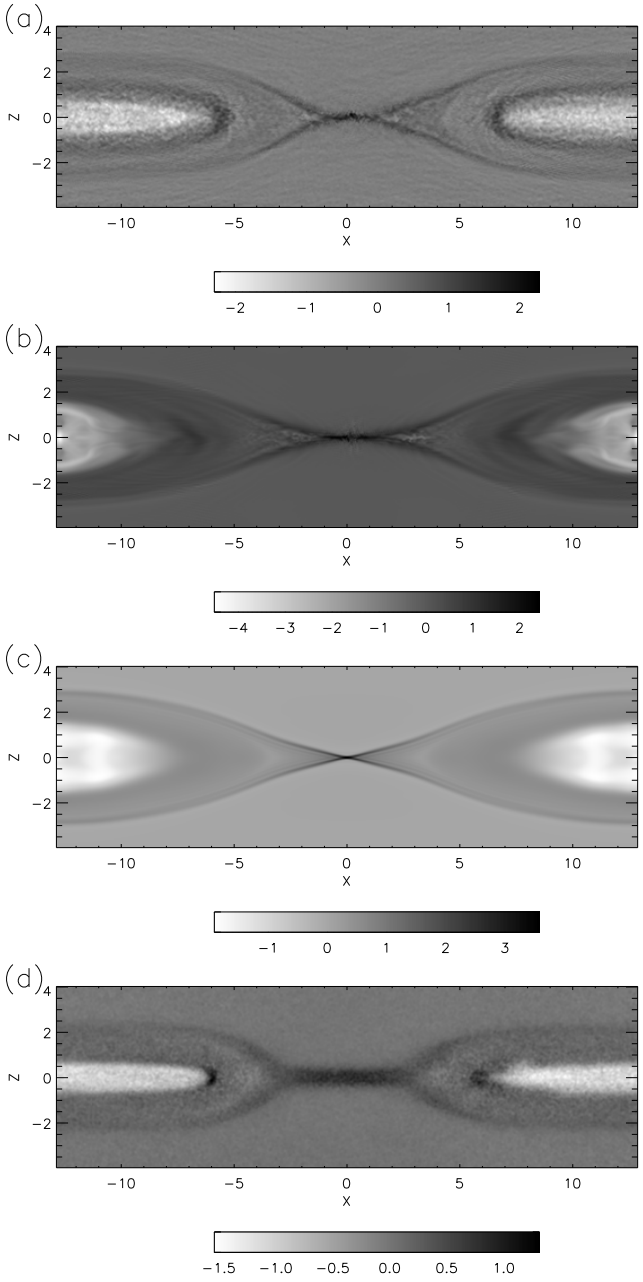

Figure 6. The electron out-of-plane current for different types of simulations: (a) hybrid, (b) Hall MHD, (c) Hall MHD with $m_e = 0$, and (d) full particle.

The electron current sheet for the full particle case in Figure 6d is broader than the other nonzero electron mass cases by about a factor of 2 in each direction. This broadening is due to the way in which c/ω_{pe} effects in Ohm's law are treated in the hybrid and Hall MHD simulations. In the fluid electron simulations, $c/\omega_{pe} = c(4\pi n_o e^2/m_e)^{-1/2}$ is a free parameter which is constant in space with $n_o = 1$ in normalized units, where n_o is defined as the initial current sheet density minus the lobe density. In order to use fast Fourier transforms to unfold $\mathbf{B}'$ into $\mathbf{B}$, where $\mathbf{B}'$ is defined in (11), c/ω_{pe} must be a constant in space. In reality, however, n varies in space and early into the reconnection process, the initial current sheet is eaten away, and lobe plasma with $n_{\rm lobe} = 0.2$ begins to reconnect. At this point in the full particle simulation, c/ω_{pe} near the x line has increased from its initial value by a factor of $\sqrt{n_o/n_{\rm lobe}} \approx 2$, which explains the difference in the electron current sheet. However, even with this factor of 2 increase in c/ω_{pe} in the full particle simulation, the reconnection rate differs only insignificantly from the Hall MHD and hybrid simulations, as was shown in Figure 1.

6. Effect of Whistlers on Electron Dynamics

From the section 5, it is clear that the process which breaks the frozen-in constraint in the very narrow electron layer has no impact on the reconnection rate, consistent with previous studies [*Biskamp et al.,* 1997; *Shay and Drake,* 1998; *Hesse et al.,* 1999]. The underlying physics is linked to the different dispersion character of the whistler and Alfvén waves. In all of the simulations which include the Hall effect and where there is no strong axial guide field, the structure of the electron dissipation region is controlled by whistler rather than Alfvén dynamics because this region has an intrinsic-scale length which is well below the ion inertial length, c/ω_{pi}. The electron dissipation region is defined as the area close to the x line, where the electrons are not frozen-in. The quadratic dispersion character of the whistler wave ($\omega \sim k^2$) leads to an increase in the phase speed with decreasing scale size and therefore to an increase in the velocity at which the electrons can be ejected from the x line as the scale size of the electron dissipation region decreases. The consequence is that in contrast to the resistive MHD scaling in (1), the whistler dynamics lead to an inflow velocity which is independent of the width of the electron dissipation region. This can be shown by carrying out a Sweet-Parker-like analysis of the electron dissipation region using the whistler equations.

We take the width of the layer in the inflow (z) direction, δ, to be controlled by an unspecified mechanism which breaks the electron frozen-in condition

and the length in the outflow (x) direction to be L. In the whistler regime the electrons are frozen-in to the magnetic field, and the ion motion can be neglected. The resulting dynamical equations in a two-dimensional(2-D) system are [*Biskamp et al.*, 1997]

$$\frac{\partial \psi}{\partial t} + \mathbf{v}_e \cdot \nabla \psi = 0, \quad \frac{\partial B_y}{\partial t} - \mathbf{B} \cdot \nabla v_{ey} = 0 \qquad (20)$$

$$\mathbf{v}_e = -\frac{c}{4\pi n e}(\nabla B_y \mathbf{\times} \hat{\mathbf{y}} + \hat{\mathbf{y}} \nabla^2 \psi) \qquad (21)$$

where $\mathbf{B} = \hat{\mathbf{y}} \mathbf{\times} \nabla \psi + B_y \hat{\mathbf{y}}$. The outflow velocity follows from the x component of (21), $v_{ex} \sim cB_y/(4\pi n e \delta)$. The out-of-plane field B_y arises from bending the in-plane field. The source ($\sim B_x v_{ey}/L$) acts for a time of the order of the convection time out of the dissipation region $\sim L/v_{ex}$ so $B_y \sim B_x v_{ey}/v_{ex}$. Combining these relations and eliminating v_{ey} using (21), we obtain $B_y \sim B_x$, $v_{ex} \sim v_{ey}$ and the electron outflow velocity $v_{ex} \sim \Omega_e \delta_e^2/\delta$, which is the whistler analogue of the Alfvén outflow condition in MHD. The important point is that this outflow velocity scales inversely with the width of the dissipation region. Applying continuity ($v_{ex}\delta \sim v_i L$), the inflow velocity is given by

$$v_{\rm in} \sim \frac{1}{L}\delta_e^2 \Omega_e. \qquad (22)$$

The reconnection rate is independent of δ and therefore the mechanism by which the electron frozen-in condition is broken. The reconnection rate remains finite even as $\delta \to 0$.

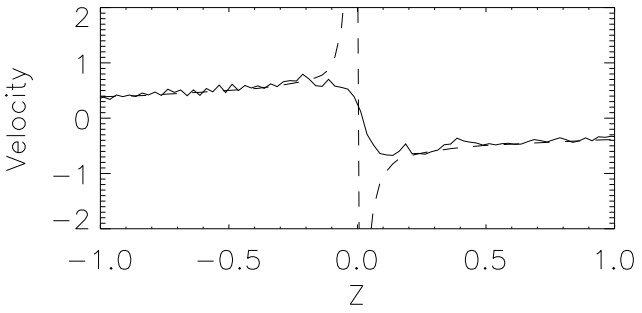

Figure 7. A cut along $\hat{\mathbf{z}}$ of the electron inflow velocity (solid line) and the electron $\mathbf{E}\times\mathbf{B}$ velocity (dashed line). The electron dissipation region begins where the two diverge.

We now use the above physical arguments to examine the electron dissipation region in the hybrid runs in Figure 3. In these runs, the frozen-in constraint for the electrons is finally broken by electron inertia, so the width of the dissipation region should scale like c/ω_{pe}. The electron dissipation region, defined as the region near the x line where the frozen-in constraint for the electrons is finally broken, is roughly coincident with the intense electron current sheet, an example of which is shown in Figure 4a. In this case the electron dissipation region has a width along z of $\approx 2\, c/\omega_{pe}$ and a length of $\approx 10\, c/\omega_{pe}$, with $c/\omega_{pe} = 0.1$ in normalized units. The width along z can be determined more precisely by comparing the inflow electron velocity with the $\mathbf{E}\times\mathbf{B}$ drift speed along z. When the two diverge, the electrons are no longer frozen-in. Figure 7 is a cut along z of the electron inflow speed (solid line) and the $\mathbf{E}\times\mathbf{B}$ drift speed (dashed line) for a hybrid run with $m_e/m_i = 1/64$ on a 1024×512 grid. The $\mathbf{E}\times\mathbf{B}$ drift speed is defined as $v_{Ez} = E_y/B_x$ in normalized coordinates. In making these plots, the values have been averaged over the range $x = [-0.25, 0.25]$ in order to reduce noise. In all of the hybrid simulations at this point in the reconnection process, $E_y \approx 0.20$. In this case, the electron dissipation region extends from $z \approx \pm 0.16$. Figure 8a is a plot of δ versus c/ω_{pe} from the four different hybrid simulations. The dashed line has a slope of 0.93. Clearly, the width of the electron dissipation region scales with c/ω_{pe}.

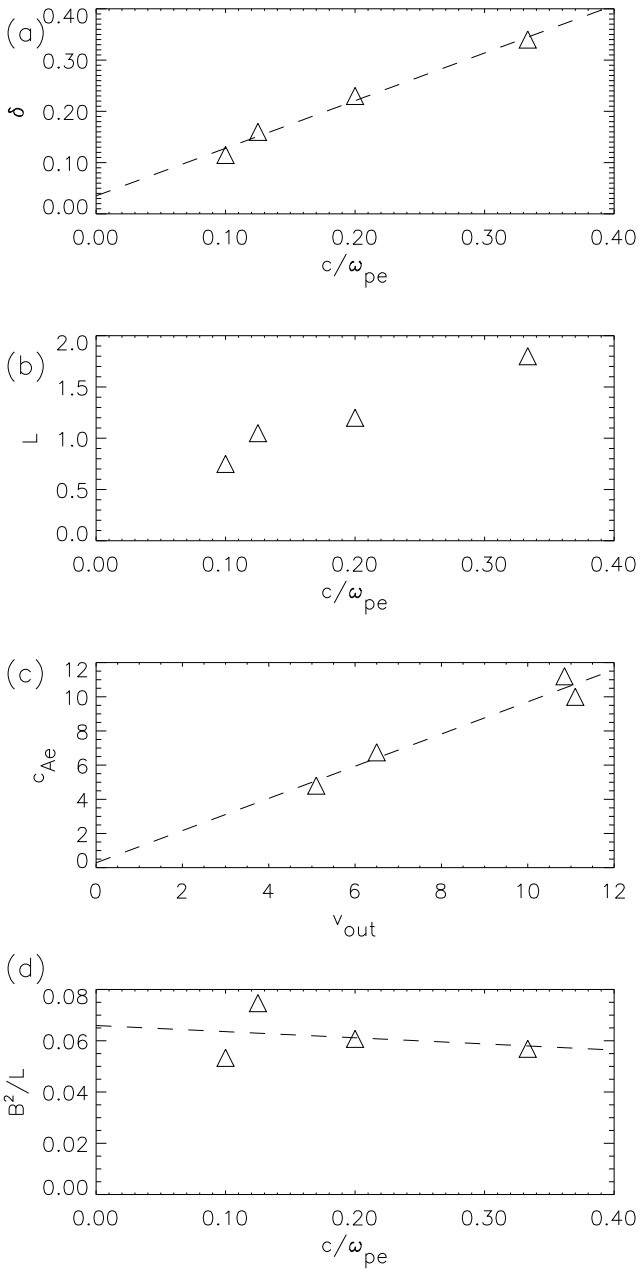

Figure 8. The response of the inner electron layer to changes in electron mass: (a) width along $\hat{\mathbf{z}}$ of the electron dissipation region versus c/ω_{pe}, (b) length along $\hat{\mathbf{x}}$ of the electron dissipation region versus c/ω_{pe}, (c) electron Alfvén speed versus electron outflow speed, and (d) B_x^2/L versus c/ω_{pe}.

Along the outflow direction ($\hat{\mathbf{x}}$), the length of the dissipation region is determined by the location of maximum electron outflow. Assuming a rectangular dissipation region, the electron outflow must be a maximum at the outflow edge of the electron dissipation region in order to conserve total mass. Beyond the electron dissipation region, the electron flow diverges, decreasing the outflow speed. Figure 9 is a cut along $\hat{\mathbf{x}}$ of the electron outflow speed for the largest and smallest electron mass runs in Figure 3. These values have been averaged for three grid points around $z = 0$ to reduce noise. Not only does the length along $\hat{\mathbf{x}}$ of the electron dissipation region increase significantly as the electron mass is increased, but the maximum outflow speed decreases considerably. In Figure 8b, this length along x is plotted versus c/ω_{pe}, and there is clearly a strong correlation between the two.

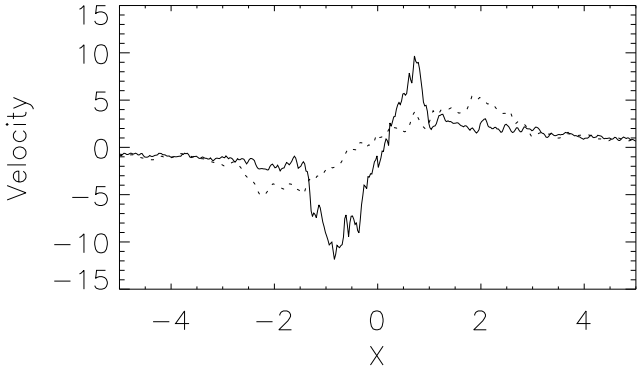

Figure 9. Slices of electron outflow speeds along x for two different electron masses: $m_e/m_i = 1/100$ (solid line) and $m_e/m_i = 1/9$ (dotted line).

Setting $\delta = c/\omega_{pe}$ in the Sweet-Parker analysis of the electron dissipation region, the electron outflow speed is

$$v_{\rm out} = v_{ex} \sim c_{Ae} = \frac{B_x}{\sqrt{4\pi n m_e}}, \qquad (23)$$

where B_x is the inflow magnetic field. That is, B_x is measured at the location in Figure 7 where the electron $\mathbf{E}\times\mathbf{B}$ drift speed diverges from the electron inflow speed. The density n inside the electron dissipation region is 0.2 because at this point in time it is lobe magnetic flux which is reconnecting. Figure 8c is a plot of the maximum electron outflow ($v_{\rm out}$) versus c_{Ae}. The electron outflow speed scales like the electron Alfvén speed, which is the primary reason that the reconnection rate is independent of the electron mass. As the electron mass decreases and the electron dissipation region gets narrower, the electron outflow

speed increases and compensates. There is no electron bottleneck.

A final check of the scaling laws for the electron dissipation region can be done by comparing the inflow rate given by the geometry of the dissipation region in (22) with the **E×B** drift speed, cE_y/B_x, where E_y is the measured reconnection electric field. Equating the two yields,

$$E_y \sim \frac{B_x^2}{L}\left[\frac{1}{4\pi ne}\right]. \quad (24)$$

All of the values in the bracket in the right-hand side are unchanged between the simulations. Because the reconnection electric field remains constant as the electron mass is varied, B_x^2/L should also remain constant. Figure 8d is a plot of B_x^2/L versus c/ω_{pe}. The best fit line (dashed line) is almost horizontal, confirming the basic scaling relations.

The involvement of whistler dynamics in kinetic reconnection has further implications for modeling high-temperature reconnection. Specifically, it implies that during fast, whistler mediated reconnection, resistivity is not adequate to balance the reconnection electric field in the electron dissipation region unless the resistivity is excessive. In other words, in a Hall MHD or Hybrid simulation of reconnection where the only mechanism to break the frozen-in constraint is a relatively small value of constant resistivity, the electron dissipation region will collapse down to the grid scale.

In order to illustrate the collapse, we examine the conditions required for resistive drag to balance the reconnection electric field, i.e.,

$$E_y \sim \eta J_y. \quad (25)$$

We will show that (25) cannot be satisfied during whistler mediated reconnection unless η becomes extremely large. The reconnection electric field E_y also determines the inflow speed of the electrons into the electron dissipation region due to their **E×B** motion:

$$E_y \sim \frac{v_{\rm in}}{c} B_x, \quad (26)$$

where B_x is the magnetic field at the inflow edge of the electron dissipation region. The Sweet-Parker physical scaling arguments used to derive (22) are valid, so that $v_{\rm in} \sim (\delta/L)(\delta_e^2\Omega_e/\delta)$. In all of the simulations in this study, δ appears to scale roughly with L such that δ/L is of the order of 1/5. Substituting, we find that

$$\frac{\eta c^2}{4\pi}\frac{1}{\delta^2} \sim \frac{\delta_e^2\Omega_e}{\delta^2}\ \frac{1}{5}. \quad (27)$$

The left-hand side of the equation is the rate of diffusion due to the constant resistivity, and the right-hand side is the frequency associated with the whistler waves which accelerate plasma away from the electron dissipation region. Both sides of the equation scale like $1/\delta^2$, so even as $\delta \to 0$, the resistive diffusion rate will not be able to overpower the whistler frequency unless $\eta c^2/(4\pi) \sim 1/5\,\delta_e^2\Omega_e$, which can be rewritten $\nu_{ei} \sim \Omega_e/5$, using $\eta \equiv m_e\nu_{ei}/(ne^2)$. For such a value of the electron collision rate, electrons are nearly unmagnetized everywhere. In MHD, on the other hand, the right-hand side of (27) scales at most like c_A/δ so that as δ becomes small the resistive diffusion will always overpower the Alfvén wave and balance the reconnection electric field.

In summation, the high-speed whistler waves present at small scales render classical resistivity ineffective at balancing the reconnection electric field during whistler-mediated reconnection. In order to balance this electric field with a resistive model, a current dependent resistivity or a higher-order resistivity (∇^n with $n \geq 4$) is needed. This conclusion is consistent with resistive Hall MHD simulations of the GEM reconnection challenge problem [*Birn and Hesse,* this issue].

7. Role of the Ions

The dynamics of the electrons in the inner electron current sheet do not control the rate of reconnection. This rate is instead determined by the larger-scale ion dynamics [*Shay et al.,* 1999]. Changing from fluid to particle ions leads to substantial changes in the structure of the ion acceleration region just downstream of the x line. The surprise is that these differences are not reflected in differences between the rates of magnetic reconnection in the two models. Figure 10 compares flows and the particle density for a hybrid simulation and a fluid simulation, both with $m_e/m_i = 1/25$ on a 512×256 grid. The Hall MHD simulation is on the left and the hybrid simulation is on the right, with plots of ion bulk flow velocities (Figure 10a), ion out of plane current(Figure 10b), and density(Figure 10c). In the fluid ion case, all of the ion flows are much more intense and are generally more spatially localized. For example, the ion outflow channel away from the dissipation region is almost twice as wide in the hybrid case, with the maximum ion outflow being about half that of the

fluid model. These two changes offset each other, making the flux out about the same, which is why the reconnection rate is unchanged between the two simulations as was shown in Figure 1. Similarly, the out-of-plane current in Figure 10 is less intense and has less small-scale structure in the case with particle ions. The scales for the particle ions are increased due to orbit effects, which tend to mix the ions spatially and generally smooth the ion moments [*Laval et al.,* 1966; *Dungey,* 1988; *Burkhart et al.,* 1990; *Shay et al.,* 1998]. These finite orbit effects are of course not present in the Hall MHD simulations which allow the ion flows to contract down to smaller spatial scales.

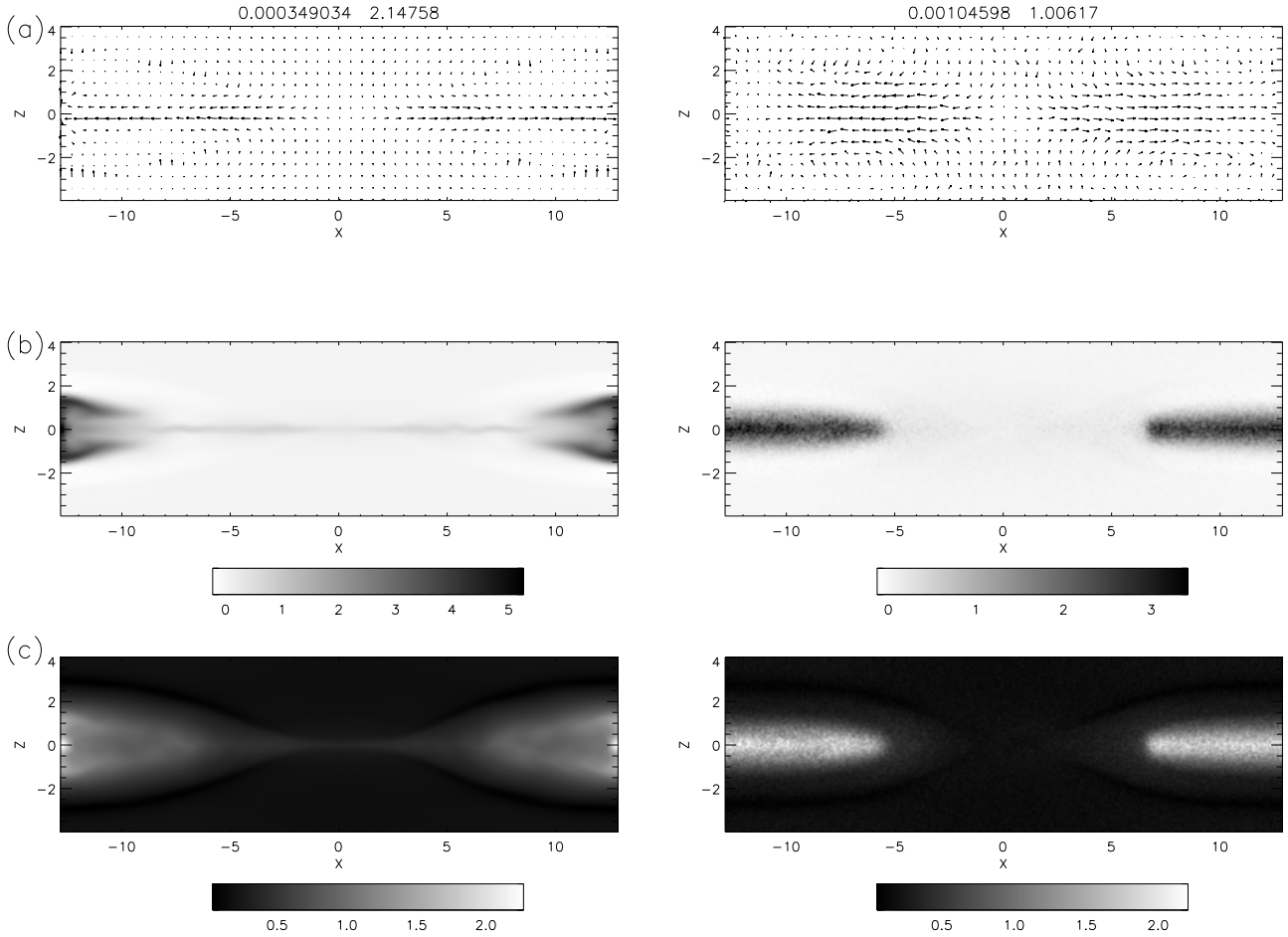

Figure 10. Comparison of fluid ions with particle ions: A Hall MHD simulation (left) and a hybrid simulation (right): (a) ion in-plane velocities, (b) ion out-of-plane current, and (c) density.

8. Density Depletion Layer

In simulations of reconnection which include Hall physics, circular loops of current form near the separatrices which create the quadrupole structure of the out-of-plane magnetic field. These loops of current, which are effectively electron flows, drag the magnetic field in such a way that the in-plane magnetic field compresses at the separatrices, giving rise to a band of increased magnetic pressure with a thickness of about a c/ω_{pi}. Although at this scale the electrons feel no magnetic pressure, the unmagnetized ions do, and these ions are expelled perpendicular to the field

lines, causing a "density depletion layer."

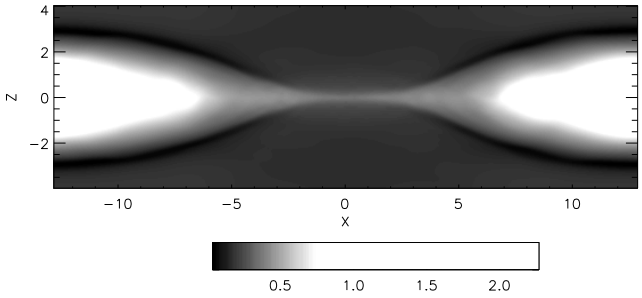

Figure 11. Density for a Hall MHD run with $m_e/m_i = 1/25$. Note the dark bands of low density.

Figure 11 is a plot of the density for the $m_e/m_i = 1/25$ Hall MHD simulation. The color table has been skewed to bring out variations in lower values of density. The black wings which follow the shape of the separatrices are the region of interest. The density in these bands is as low as 0.03, very much reduced from the initial lobe density of 0.2. In the hybrid and full particle simulations, these density depletion layers are also present but are somewhat weaker due probably to finite ion and electron larmor radius effects: In the hybrid case, the density decreases to 0.1, and in the full particle case, the density decreases to 0.15. Coincident with this band of low density is an increase in magnetic pressure, which is shown in Figure 12, whose color table has also been skewed to highlight this region. This density depletion layer causes numerical problems in fluid simulations because when the density becomes very small, it can easily become negative due to the finite accuracy of the time-stepping scheme for the density equation. Once the density becomes negative, the simulation soon crashes. This density depletion layer does not pose a numerical problem in the hybrid and full particle simulations because the density cannot go negative in a particle-in-cell code.

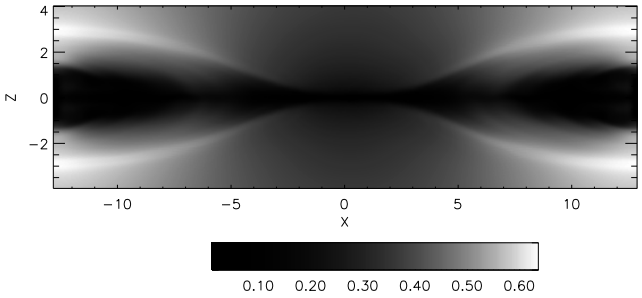

Figure 12. Magnetic pressure for a Hall MHD run with $m_e/m_i = 1/25$. Note the white bands of high-magnetic pressure.

The thickness of the density depletion layer is of the order of c/ω_{pi}, which is the first clue that Hall physics rather than MHD physics is responsible for this phenomenon. In this region near the separatrix, the in-plane flows are dominated by high velocity electron streams along the field lines which are part of the Hall current system. These Hall currents can be visualized by looking at contours of B_y, which are stream functions of the in-plane currents because $\mathbf{J} = c/4\pi\nabla\times\mathbf{B}$. Figure 13 shows the contours of B_y for the same run as Figure 11. Only the upper-right quadrant of the simulation is shown. The very thick black line is the separatrix, and the x line is at $(x, z) = (0, 0)$. These Hall currents have been seen in a large number of simulations of reconnection, beginning with the work of Terasawa [*Terasawa*, 1983].

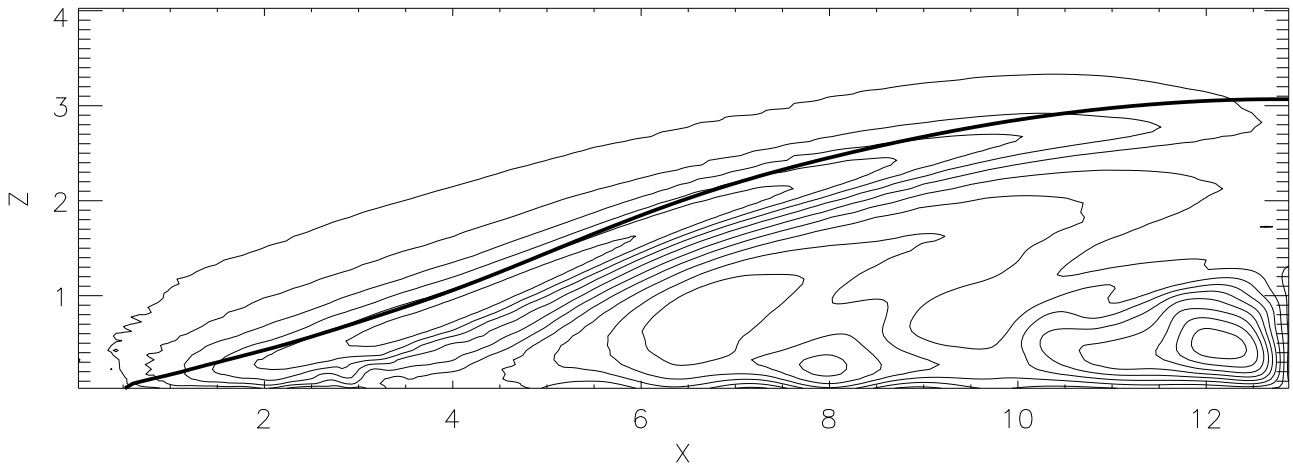

Figure 13. The contours of B_y, which are current streamlines. The separatrix is the thick line. Note the currents nearly parallel to **B** on either side of the separatrix.

To elucidate the physics responsible for the increase in magnetic pressure, we ignore the ion flow for the time being and assume that these Hall currents are actual electron flows; that is, we examine this system in the context of electron MHD. Very close to the x line, the electrons cross the separatrix and then turn the corner and flow along field lines just inside of the separatrix. Starting around $x = 6$, the electrons begin to flow back toward the x line along the field lines, forming a current loop which straddles the separatrix. This circular flow pattern generates the quadrupole B_y seen in Figure 2f. In the region, $x > 6$, the frozen-in upward (along $-\hat{\mathbf{z}}$) flow of the electrons as they turn around drags the magnetic field upward. These outward moving magnetic field lines press up against the magnetic field lines outside of the separatrix, causing an increase in the in-plane magnetic field and thus an increase in magnetic pressure. In an MHD system, such a local increase in magnetic pressure would be impossible because magnetosonic waves would quickly flatten out any increases in magnetic pressure. At the small spatial scales associated with this Hall current loop, however, the electrons experience no force associated with magnetic pressure, allowing the system to remain in quasi-equilibrium even with a local increase in magnetic pressure. In electron MHD simulations of reconnection where there is no magnetic pressure force anywhere, this magnetic pressure spike can become very large indeed, being equal to twice the lobe magnetic pressure. In the context of electron MHD, these current loops and the subsequent compression of the in-plane magnetic field are generated by whistler waves propagating almost perpendicular to the magnetic field, which can be shown with a simple linear perturbation model. In the more realistic case where the ion flows are not negligible, one obtains essentially the same physics by jumping to the local moving frame of the ions.

This magnetic pressure spike near the separatrices is manifested as an electric field which expels the ions. To see this, we examine Ohm's law near the separatrices where the electrons are frozen-in:

$$\mathbf{E} = -\frac{\mathbf{v}_e}{c}\mathbf{\times B} \approx \frac{1}{4\pi ne}\left[-\frac{\nabla B^2}{2} + \mathbf{B}\cdot\nabla\mathbf{B}\right], \qquad (28)$$

where the ion flow has been ignored compared to the electron flow. The local increase of magnetic pressure is manifested as an electric field which points away from the magnetic pressure peak, perpendicular to the in-plane magnetic field. Because the ions are not frozen-in in this narrow region which scales with c/ω_{pi}, they can respond to this electric field by flowing away from the magnetic pressure peak, perpendicular to the magnetic field lines. This flow depletes the density until force balance is achieved such that

$$\frac{B^2}{8\pi} + P_i + P_e \approx 0. \qquad (29)$$

9. Comparison with Observations

The theory of fast, Hall reconnection examined in this study raises two clear observational questions, Are the reconnection rates comparable to those inferred from magnetosphere observations and are there any signatures of fast, Hall reconnection that would be discernible from single satellite data? In this section, we examine both of these issues.

The average electric field in these simulations is ≈ 0.25 in normalized units, which corresponds to an inflow speed of $v_{\rm in} \approx 0.1 c_A$, where c_A is the Alfven speed in the region of inflowing plasma upstream of the dissipation region. Is this reconnection rate large enough to describe reconnection rates inferred from magnetosphere observations?

If reconnection at the magnetopause is driving flow across the polar cap, this $0.1 c_A$ inflow speed should be large enough to predict the cross polar cap potential. The Alfvén velocity on the magnetosphere side of the magnetopause can be 50 times larger than c_A in the solar wind, so that the reconnection rate at the magnetopause is almost assuredly limited by the solar wind Alfvén speed. Taking $B \sim 40$ nT and $n \sim 10$ cm^{-3}, the Alfvén speed is 280 km s^{-1}. Using $v_{\rm in}/c_A \approx 0.1$, the reconnection electric field is 0.7 mV m^{-1}, which is comparable to observational estimates of the electric field tangential to the magnetopause [*Sonnerup et al.,* 1990]. Taking the length of the magnetic merging line to be around 12 R_E [*Scurry et al.,* 1994], the cross-polar potential drop is ≈ 40 kV, which is of the same order as the measured 50 kV average polar cap potential drop [*Reiff and Luhmann,* 1986].

The reconnection rates found are also consistent with timescales associated with the release of magnetic energy stored in the lobes during the expansion phase of substorms. Taking a lobe density of 0.05 cm^{-3}, $B \sim 15$ nT, we calculate that $c_A = 1500$ km s^{-1} and that the inflow velocity into the x line is of order 150 km s^{-1}. In 10 min a significant fraction of the lobe flux can be reconnected.

Are there any particular signatures, besides the rate of reconnection which could be used to test the validity of this theory? One of the most obvious is the quadrupole out-of-plane magnetic field induced by the reconnection process. This magnetic field continues to manifest itself in more realistic models(B. N. Rogers, J. F. Drake, and M. A. Shay, The onset of turbulence in three-dimensional collisionless magnetic reconnection, submitted to *Geophysical Research Letters,* 2000)(hereinafter referred to as Rogers et al., submitted manuscript, 2000). As only individual satellite data is available for the magnetic field, it is very difficult to determine if a coherent quadrupole structure has been established around a reconnection point in the magnetosphere. However, large field-aligned electron currents near the dissipation region would be a good indication of whistler-mediated reconnection. In addition, these field-aligned currents should be coincident with a decrease in the density associated with the density depletion layer. Such a signature should be discernible with current satellite data.

10. Conclusion

Recently, a model of collisionless reconnection has emerged which relies on the dynamics of whistler waves due to the Hall term in the kinetic Ohm's law (10) to facilitate fast reconnection. In order to test this model and determine the minimum physics necessary to produce realistic reconnection rates, a series of simulations were performed using Hall MHD, hybrid, and full particle codes. The results show conclusively that the Hall term is the minimum physics necessary to achieve realistic reconnection rates. As long as the Hall term is included, the gross reconnection rates are the same, whether the code is full particle, hybrid, or Hall MHD.

In addition, the reconnection rate is shown to be independent of electron mass. Owing to the quadratic dispersion character of whistler waves, the outflow speed of the electrons scales like the electron Alfvén speed. As the electron mass is reduced, the electron outflow merely increases to compensate, eliminating any bottleneck of electrons which could limit the reconnection rate. In fact, when $m_e = 0$, the electron dissipation region simply collapses down to the grid scale, with no effect on the gross reconnection rate.

Also owing to whistler physics, a density depletion layer forms just outside the separatrices where a pile-up of magnetic flux due to the Hall current loops expels unmagnetized ions. In simulations with fluid ions, this decrease in density is quite strong and can cause numerical problems. The observation of such a depletion layer coincident with strong **B**-parallel electron flows during satellite crossing of the outflow region during magnetic reconnection in the magnetosphere would confirm the importance of non-MHD physics during collisionless magnetic reconnection.

Although the results from this study are very

promising, there remain unanswered questions about the generality of the results. Specifically, the effects of a guide field along the y direction and the addition of a third dimension need to be examined. When a large, spatially constant guide field B_y is added to the reconnection configuration, whistlers are replaced by kinetic Alfvén waves as the dominant dynamical ingredient at the scales of the dissipation region. In the kinetic Alfvén regime, $\rho_s \equiv \sqrt{T_e/m_i}/(eB_y/m_ic)$ replaces c/ω_{pi} as the relevant scale size of the dissipation region [*Kleva et al.,* 1995; *Drake,* 1995]. Although initial results indicate that the presence of a guide field does not slow the reconnection rate significantly [*Kleva et al.,* 1995; *Pritchett,* this issue], a thorough investigation needs to be done.

When a third dimension is added to reconnection simulations, the intense electron current sheets become electron kelvin-helmholtz unstable [*Drake et al.,* 1997]. The density variation at the separatrix can also be unstable to the lower hybrid instability, and the kinetic kink instability may cause large-scale perturbations to the current sheet [*Zhu and Winglee,* 1996; *Pritchett et. al.,* 1996; *Büchner and Kuska,* 1997]. The perturbations associated with these instabilities could widen the current sheet and wash out small-scale effects such as the density depletion layer. However, initial results indicate that even though turbulence can develop in three dimensional(3-D) reconnection, whistlers remain fundamental to the reconnection process, and the gross reconnection rate is unchanged. Therefore the quadrupole structure of the induced B_y remains, though turbulent flows strongly modulate the crisp structures seen in 2-D (Rogers et al., submitted manuscript, 2000). The density depletion layer similarly survives, although it is shredded by fluctuations associated with the lower hybrid drift instability (Rogers et al., submitted manuscript, 2000).

Acknowledgments. This work was supported by NSF grants ATM-9625242 and ATM-9713271, and NASA grants NAG5-6190 and NAG5-8459.

Janet G. Luhmann thanks the referees for their assistance in evaluating this paper.

References

Birn, J., and M. Hesse, Geospace Environment Modeling (GEM) magnetic reconnection challenge: Resistive tearing, anisotropic pressure, and Hall effects, *J. Geophys. Res.,* this issue.

Biskamp, D., Magnetic reconnection via current sheets, *Phys. Fluids, 29,* 1520, 1986.

Biskamp, D., and U. Bremer, Dynamics and statistics of inverse cascade processes in 2D magnetohydrodynamics turbulence, *Phys. Rev. Lett., 72,* 3819, 1993.

Biskamp, D., E. Schwarz, and J. F. Drake, Two-fluid theory of collisionless magnetic reconnection, *Phys. Plasmas, 4,* 1002, 1997.

Büchner, J., and J. P. Kuska, Numerical simulation of three-dimensional reconnection due to the instability of collisionless current sheets, *Adv. Space Res., 19,* (12), 1817, 1997.

Burkhart, G. R., J. F. Drake, and J. Chen, Magnetic reconnection in collisionless plasmas: Prescribed fields, *J. Geophys. Res., 95*, 18,833, 1990.

Cai, H. J., D. Q. Ding, and L. C. Lee, Momentum transport near a magnetic X line in collisionless reconnection, *J. Geophys. Res., 99*, 35, 1994.

Drake, J. F., Magnetic reconnection: A kinetic treatment, in *Physics of the Magnetopause, Geophys. Monogr. Ser.,* vol. 90, edited by P. Song, B. U. Ö., Sonnerup, and M. F. Thomsen, p. 155, AGU, Washington, D.C., 1995.

Drake, J. F., D. Biskamp, and A. Zeiler, Breakup of the electron current layer during 3-D collisionless magnetic reconnection, *Geophys. Res. Lett., 24*, 2921, 1997.

Dungey, J. W., Noise-free neutral sheet, in *Proceedings of an International Workshop in Space Plasma,* vol. II, *Eur. Space Agency Spec. Publ., ESA SP-285,* 15, 1988.

Hesse, M., and D. Winske, Electron dissipation in collisionless magnetic reconnection, *J. Geophys. Res., 103*, 26,479, 1998.

Hesse, M., K. Schindler, J. Birn, and M. Kuznetsova, The diffusion region in collisionless magnetic reconnection, *Phys. Plasmas, 6*, 1781, 1999.

Horiuchi, R., and T. Sato, Particle simulation study of collisionless driven reconnection in a sheared magnetic field, *Phys. Plasmas, 4,* 277, 1997.

Kleva, R. G., J. F. Drake, and F. L. Waelbroeck, Fast reconnection in high temperature plasmas, *Phys. Plasmas, 2,* 23, 1995.

Kuznetsova, M., M. Hesse, and D. Winske, Kinetic quasi-viscous and bulk flow inertia effects in collisionless magnetotail reconnection, *J. Geophys. Res., 103*, 199, 1998.

Laval, G. R., R. Pellat, and M. Vuillemin, Instabilities electromagnetiques des plasmas sans collisions, *Plasma Phys. Controlled Nucl. Fusion Res., 2*, 259, 1966.

Lyons, L. R., and D. C. Pridemore-Brown, Force balance near an X line in a collisionless plasma, *J. Geophys. Res., 95*, 20,903, 1990.

Ma, Z. W., and A. Bhattacharjee, Fast impulsive reconnection and current sheet intensification due to electron pressure gradients in semi-collisional plasmas, *Geophys. Res. Lett., 23,* 1673, 1996.

Mandt, M. E., R. E. Denton, and J. F. Drake, Transition to whistler mediated magnetic reconnection, *Geophys. Res. Lett., 21,* 73, 1994.

Nakamura, M. S., M. Fujimoto, and K. Maezawa, Ion dynamics and resultant velocity space distributions in the course of magnetotail reconnection, *J. Geophys. Res., 103*, 4531, 1998.

Parker, E. N., Sweet's mechanism for merging magnetic fields in conducting fluids, *J. Geophys. Res., 62*, 509, 1957.

Pritchett, P. L., Geospace Environment Modeling(GEM) reconnection challenge: Simulations with a full particle electromagnetic code, *J. Geophys. Res.,* this issue.

Pritchett, P. L., F. V. Coroniti, and V. K. Decyk, Three-dimensional stability of thin quasi-neutral current sheets, *J. Geophys. Res., 101,* 27,413, 1996.

Reiff, P. H., and J. G. Luhmann, Solar wind control of the polar cap voltage, in *Solar-Wind Magnetosphere Coupling*, edited by Y. Kamide and J. A. Slavin, pp. 453-476, Terra Sci., Tokyo, 1986.

Scurry, L., C. T. Russell, and J. T. Gosling, A statistical study of accelerated flow events at the dayside magnetopause, *J. Geophys. Res., 99*, 14,815, 1994.

Shay, M. A., and J. F. Drake, The role of electron dissipation on the rate of collisionless magnetic reconnection, *Geophys. Res. Lett., 25*, 3759, 1998.

Shay, M. A., J. F. Drake, R. E. Denton, and D. Biskamp, Structure of the dissipation region during collisionless magnetic reconnection, *J. Geophys. Res., 103*, 9165, 1998.

Shay, M. A., J. F. Drake, B. N. Rogers, and R. E. Denton, The scaling of collisionless, magnetic reconnection for large systems, *Geophys. Res. Lett., 26*, 2163, 1999.

Sonnerup, B. U. Ö., Magnetic field reconnection, in *Solar System Plasma Physics,* vol. 3, edited by L. J. Lanzerotti, C. F. Kennel, and E. N. Parker, 3, p. 46, North-Holland, New York, 1979.

Sonnerup, B. U. Ö., I. Papamastorakis, G. Paschmann, and H. Lühr, The magnetopause for large magnetic shear: Analysis of convection electric fields from AMPTE/IRM, *J. Geophys. Res.*, *95*, 10,541, 1990.

Sweet, P. A., in Electromagnetic Phenomena in Cosmical Physics, edited by B. Lehnert, p. 123, Cambridge Univ. Press, New York, 1958.

Terasawa, T., Hall current effect on tearing mode instability, *Geophys. Res. Lett., 10*, 475, 1983.

Vasyliunas, V. M., Theoretical models of magnetic field line merging, *Rev. Geophys. 13*, 303, 1975.

Zhu, Z., and R. M. Winglee, Tearing instability, flux ropes, and the kinetic current sheet kink instability in the Earth's magnetotail: A three-dimensional perspective from particle simulations, *J. Geophys. Res., 101,* 4885, 1996.

R. E. Denton, Department of Physics and Astronomy, Dartmouth College, Hanover, NH 03755-3528.

J. F. Drake, B. N. Rogers, and M. A. Shay, Institute for Plasma Research, University of Maryland, College Park, MD 20742. (shay@glue.umd.edu; drake@glue.umd.edu; rogers@glue.umd.edu)

Received August 23, 1999; revised November 22, 1999; accepted December 22, 1999.

This preprint was prepared with AGU's LaTeX macros v5.01. File reprint formatted February 16, 2000.